Theoretical investigation of a direct-contact humidification-dehumidification desalination system

Alejandro Alvarez[a], Francisco Carranza[a,b], Ivett Zavala[a], Daniel Sauceda[a],*

[a]*Renewable Energy Laboratory, Applied Physics Division, Centre for Scientific Research and Higher Education of Ensenada (CICESE), Ensenada, Hwy. Ensenada – Tijuana 3918, Zona Playitas, 22860 Ensenada, B.C. Mexico, Tel. +52 646 175 0500;*
emails: dsauceda@cicese.edu.mx (D. Sauceda), aalvarez@cicese.edu.mx (A. Alvarez), fcarranza@cicese.edu.mx (F. Carranza),
ivett@cicese.edu.mx (I. Zavala)
[b]*National Council for Science and Technology (CONACYT), Insurgentes Sur Ave. 1582, Mexico City 03940, Mexico*

A B S T R A C T

In this paper, a numerical investigation of a direct-contact humidification-dehumidification desalination system is presented. The system functions in an open loop for both the air and the water and does not have packing materials inside the humidifier and dehumidifier. The air is humidified by spraying hot seawater into it and then dehumidified by spraying cold freshwater. Both processes occur in a counterflow arrangement. The mass and energy conservation equations at steady-state conditions were solved through a finite difference scheme. During the solution, the properties of the fluids were evaluated for each discrete element. The influence of the geometry was also examined through the variation of the humidifier and dehumidifier height ratio. From the results, it was observed that for a fixed geometry, the freshwater production is enhanced through small droplet diameter and velocity and high seawater temperature and mass flow rate. The largest production achieved was 242.2 kg/h at a height ratio of 2.0. Increasing the height ratio was in general beneficial; however, the gains after it exceeded 1.5 were not significant. Since no attempt of heat recovery was done for this system, the gained output ratio was consistently low for all the cases analyzed. The largest value obtained was 0.58.

Keywords: Seawater desalination; Humidification; Dehumidification; Droplets; Direct contact

1. Introduction

Sustainable water and energy supplies are two most important issues that humankind must solve for the appropriate development of the current and future generations. Some parts of the world have already been facing serious challenges due to water scarcity during the last decades. Unless adequate actions are taken, such issues will continue to exist and augment. According to the United Nations, by the year 2025, about 1.8 billion people will live in regions of complete water scarcity [1]. In addition, between 3.6 and 4.6 billion will live under dangerous water stress by 2050 [2].

This situation is a consequence of the rapid growth of the population as well as due to urbanization, industrialization, expansion of agriculture, and water mismanagement. Available water resources are currently overexploited in many parts of the world. A significant part of them are also polluted. Overexploitation of ground water reserves has caused their saline concentration levels to increase, thus reducing the water quality. However, a large number of the places already facing critical water shortages are situated in coastal arid regions or in islands, with plenty of access to both

* Corresponding author.

seawater and solar radiation. In such scenarios, desalination powered by solar energy has arisen as a promising option.

The removal of salts from seawater or brackish water through the use of solar energy is considered a sustainable solution because this type of energy does not pollute, is free, and it is relatively easy to harness [3–6]. Furthermore, solar radiation can be converted to thermal energy at noticeably high efficiencies [6]. Nonetheless, the nature of solar energy makes it unsuitable to power desalination systems of large capacity at an acceptable cost. This constitutes a significant obstacle to combine it with the already well-established, thermally driven desalination technologies of multistage flash distillation (MSF), multiple effect distillation (MED), and vapor compression (VC).

Due to their principle of operation, MSF, MED, and VC consume significant amounts of energy in the form of heat, normally provided by fossil fuels. They are cost effective only for large and continuous productions of freshwater. On the other hand, for the same water demand, the popular membrane-based technology of reverse osmosis (RO) requires less energy, in the form of electricity. RO can work effectively with solar photovoltaics (PV) but at low and intermittent production rates. Moreover, the inability of RO to handle waters of high salinity plus the short useful life and prominent cost of the PV cells make such systems unappealing in many cases [7,8].

Given this context, it is clear that alternative desalination methods, more suitable to the nature of solar energy, have to be developed. Among the proposed techniques, the ones which have caught most of the attention during the last decade are solar stills (SS), membrane distillation (MD), forward osmosis (FO), and humidification-dehumidification (HD). In SS, saltwater contained in a black-painted pan is evaporated inside a shelter made of glass or translucent plastic which traps solar radiation. The steam is condensed at the ceiling of the shelter and collected by an arrangement of channels attached to the structure. SS are economical, easy to operate, and can handle waters of high salinity, though their productivity is low. To improve it, the size of the shelter has to be increased significantly and an auxiliary solar heating equipment has to be used too [9].

MD is a technology which combines evaporation and membrane separation into a single unit. By means of an external source of energy, sea or brackish water is heated and then introduced into the hot side of the unit where there is a hydrophobic membrane that only allows the passage of vapor. After crossing the membrane, the vapor gets condensed on the other side by a flowing liquid of lower temperature. As long as the membrane is the only barrier between the hot and cold streams, low temperature differences (10°C approximately) are enough to drive the process [10]. Nonetheless, current MD membranes tend to lose their hydrophobicity and get fouled during long-term operation. Furthermore, they are characterized by a relatively low permeate flux, affecting the productivity [9].

Through the preparation of a draw solution of higher concentration than seawater, FO can achieve desalination by putting both liquids into contact, only separated by a porous membrane. The osmotic pressure difference caused by the concentration of the fluids makes the solvent move across the membrane, from the lower concentration region to the higher concentration region. Afterwards, the solvent is separated from the draw solution in order to produce freshwater. External heating at low temperature is employed [11]. Despite the fact of working at a lower pressure than RO, the current scarcity of high-performance membranes and the difficulties in the separation of water from the draw solution are important drawbacks of this technology [12].

On the other hand, HD is a simple and economical desalination method. It is compact and suitable for waters of variable salinity. In an HD system, freshwater is produced by imitating the water cycle in our planet. First, seawater is evaporated through the humidification of a dry air stream. Then, in the dehumidifier, the water vapor is condensed with the assistance of a heat exchanger. The air leaving the condenser can be released to the atmosphere, creating an open-loop configuration, or reintroduced into the evaporator, forming a closed-loop configuration. Before entering the humidifier, at least one of the fluids has to be heated. It has been recommended to prioritize the heating of the water because the effect of the air temperature on the performance of the system has been found marginal [13].

Since the operating temperature is usually inferior to 100°C and the pressure is relatively close to the atmospheric pressure, inexpensive solar collectors can be employed to heat the seawater. Moreover, these operating conditions also inhibit the problems of leaking, corrosion, and scaling significantly [5,14–16]. Because there is no need to utilize membranes, intensive feedwater pretreatments are not required. Due to these advantages, HD has been proposed as the best alternative for solar energy desalination at low and medium capacities [5,17]. Furthermore, according to Kabeel et al. [18], HD is the most appropriate method for small capacity water production.

An additional benefit of HD is the fact that it can be combined with other types of desalination methods, such as RO [19], SS [20–22], and single-stage flashing evaporation [23]. Furthermore, provided that HD can also work on waste or geothermal heats, it is possible to develop energy-hybrid arrangements to assure continuous operation [16]. He et al. [24] did a thermo-economic analysis of an HD system powered by waste heat and found that the cost of the desalinated water was considerably lower than that of other solar-powered configurations due to the lower price of the equipment used.

Mahmoud et al. [25] studied a hybrid system where HD and SS desalination were used in combination with solar concentrators and PV panels, thus supplying water, heat, and electricity simultaneously. Kabeel et al. [26] analyzed an HD desalination system coupled with solar drying and found that the thermal efficiency could be improved by 29% when the recirculating air flow rate was increased. Associations with desiccant air configurations and heat pumps have also been investigated [27,28]. In all of the cases, whether energy hybrids or combinations with other desalination methods, the global performance of the systems were enhanced, thus proving the flexibility of HD.

Typical capacities of HD desalination units are lower than 1 m^3/d; nonetheless, moderately higher productions have been reported at the expense of costly solar heating installations [29]. Attempts to increase the capacity have been done through combinations of HD with other desalination techniques, as mentioned previously, or by alternative ways

in which the evaporation and condensation processes can happen. The benefit of the second approach is the inherent savings in capital cost. An efficient way to improve the seawater evaporation rate is by filling the humidifier with some type of material such as wooden packing, honeycomb paper, or plastic rings. The result is an enlargement of the contact area between the water and the air and the improvement of the evaporation rate as consequence [9,30,31].

Despite that the filling material is beneficial for the system, it also imposes a drop in pressure which should not be neglected. Robust blowers will be required, and increased capital, operation, and maintenance costs will have to be expected. Hamed et al. [25] has observed that 4.85% of the total cost of the desalination system can be saved if packing materials are not used. Operating at natural convection conditions is feasible, though productivity will decrease due to low heat and mass transfer coefficients [32–35]. Thus, in order to avoid extra costs, configurations free of packing materials have been proposed [35].

One possible way to skip the use of packing inside the humidifier consists on spraying the heated seawater into the air stream in a counterflow arrangement. The seawater is sprayed from top to bottom while the air travels in the opposite direction. In this way, the contact surface between both fluids is also enhanced without affecting the pressure considerably. Franchini et al. [36,37] investigated this possibility and concluded that no significant improvement on the production of freshwater was achieved due to the addition of packing materials, suggesting that the utilization of such components may be unnecessary. The dehumidifier they used was an air-to-water metallic heat exchanger.

Niroomand [38] also analyzed the same possibility but applied it to the dehumidifier in a crossflow arrangement. Cold water was sprayed vertically into a hot and humid air stream flowing horizontally. They concluded that the benefits of using a direct-contact dehumidifier were considerable because substantial freshwater production rates (up to 25 kg/h) were still achieved and the pressure drop, fouling, corrosion, and scaling problems associated with the use of metallic heat exchangers were avoided. Furthermore, savings in capital costs may be obtained too. Hamed et al. [25] has shown that the price of a coil heat exchanger, for instance, can represent up to 12.48% of the final cost of the system.

Given this context, it can be seen that the use of direct-contact humidifiers and dehumidifiers can be very convenient. However, to the authors' knowledge, no analysis on the performance of an HD desalination system where both the humidifier and dehumidifier do not contain packing materials has been published. Therefore, it is the objective of this investigation to study the thermal performance and operational characteristics of such a desalination system and to identify the key parameters for enhancing its production of freshwater.

Rather than working in crossflow, preference was given to a counterflow configuration inside both units (the evaporator and the condenser) because it is believed that it guarantees a longer time of contact between the water droplets and the air. For the analysis, an appropriate theoretical model based on the mass and energy balance equations was developed. Both units were geometrically discretized and

the equations solved numerically. The thermodynamic fluid properties involved in the calculations were determined for each discrete element. The results obtained from this work will also provide a basis for the design and construction of an experimental HD installation to work with solar thermal energy. Since the optimal dimensions of the desalination system will be known, a low manufacturing price is expected.

2. System description

The HD desalination system analyzed in this work is depicted in Fig. 1. The definition of each variable is listed in the nomenclature chart. Both the humidifier and the dehumidifier do not contain packing materials. At the top of the humidifier, hot seawater is sprayed uniformly in a conical way to ensure that the droplets cover the entire cross section of the cylinder. Afterwards, they fall vertically due to gravity effects. To start the process, unsaturated air from the surroundings is injected at the bottom of the column at a temperature lower than that of the seawater. In this way, a counterflow process is formed. Direct contact exists between the seawater droplets and the air.

Given the temperature difference between both fluids and the unsaturated conditions of the entering air, heat and mass transfer from the seawater droplets to the air occurs, making the temperature and humidity content of the air increase. As the droplet evaporation advances, its temperature decreases. It is assumed that none of the droplets evaporate completely; thus, the total number remains constant. They leave the unit at a higher saline concentration, called brine. Depending on the inlet conditions of both fluids and the length of the humidifying column, the air leaving the unit might or might not reach the saturation state.

In the next stage, the hot and humid air which leaves the humidifier enters the dehumidifier from the bottom. It is considered that no changes in air temperature, humidity, or flow rate between the evaporator exit and the condenser inlet take place. To ensure a counterflow configuration, cold freshwater is sprayed at the top of the dehumidifier, again in such a way that the droplets occupy the entire cross section uniformly. As the air ascends in the column, its temperature diminishes and condensation begins. Water from the air condenses on the surface of the already existing droplets, thus augmenting their mass and temperature. It is assumed
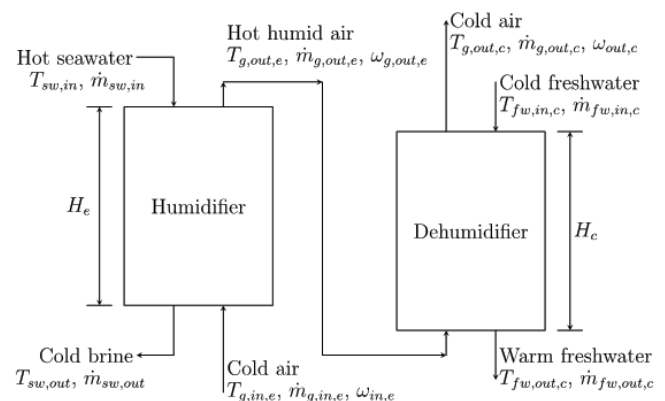

Fig. 1. Diagram of the HD desalination system investigated.

that new droplets are not formed; thus, the total number of droplets remains unchanged.

3. Mathematical model

To investigate the performance and the characteristics of operation of the desalination system shown in Fig. 1, a mathematical model based on mass and energy balance equations was developed. A set of algebraic and differential equations was obtained for the humidifier and another similar one for the dehumidifier. Starting with the humidifier, the mechanism through which mass is transferred from the seawater droplets to the air in the evaporator is convection; therefore, from a mass balance applied to an individual droplet falling vertically, the following differential equation results:

$$\frac{dm_d}{dz} = \frac{-\rho_g A_s h_m \left(\omega_{\text{int}} - \omega_g\right)}{U_d} \tag{1}$$

where m_d is the mass of the droplet, z the vertical axis, ρ_g the density of the mixture of water vapor and air (referred to as gas), A_s the surface area of the droplet, h_m the convection mass transfer coefficient for a flow near a sphere, ω_{int} the humidity ratio at the interphase droplet-air (a saturation humidity ratio at the droplet temperature was assumed), ω the gas specific humidity, and U_d the vertical velocity of the droplet. The minus sign in Eq. (1) expresses the loss of mass due to droplet evaporation. In terms of the droplet diameter D_d, Eq. (1) can be rewritten as follows:

$$\frac{dD_d}{dz} = \frac{-2\rho_g h_m \left(\omega_{\text{int}} - \omega_g\right)}{\rho_{\text{sw}} U_d} \tag{2}$$

where ρ_{sw} is the seawater density. The coefficient of mass transfer is determined by means of the Sherwood number through the next correlation [39]

$$\text{Sh} = \frac{h_m D_d}{\alpha_{w-g}} = 2 + 0.6 \times \text{R} e^{1/2} \times \text{Sc}^{1/3} \tag{3}$$

where Re is the droplet Reynolds number, Sc is the Schmidt number, and α_{w-g} is the diffusion coefficient of water vapor in air, also called mass diffusivity. Re is calculated based on the relative velocity between the droplet and the air W with the following equation:

$$\text{Re} = \frac{WD}{\upsilon_g} \tag{4}$$

where υ_g denotes the gas kinematic viscosity or momentum diffusivity. The Schmidt number is computed using the next equation:

$$\text{Sc} = \frac{\upsilon_g}{\alpha_{w-g}} \tag{5}$$

Heat is transferred from the droplet to the surrounding gas by convection and evaporation; thus, from an energy balance, the following differential equation was obtained to describe the energy transfer between the air and one droplet:

$$m_d Cp_d \frac{dT_g}{dz} + h_d \frac{dm_d}{dz} = \frac{h_h A_s \left(T_g - T_d\right)}{U_d} + h_{\text{fg}} \frac{dm_d}{dz} \tag{6}$$

where Cp_d is the droplet specific heat, T_g the gas temperature, h_d the droplet specific enthalpy, h_h the convection heat transfer coefficient, T_d the droplet temperature, and h_{fg} the enthalpy of vaporization. For the case of flow around a sphere, h_h is found as a function of the Nusselt number Nu through the next correlation [39]

$$\text{Nu} = \frac{h_h D}{\lambda_g} = 2 + 0.6 \times \text{R} e^{1/2} \times \text{Pr}^{1/3} \tag{7}$$

where λ_g is the gas thermal conductivity and Pr is the gas Prandtl number. By means of a mass balance applied to the gas, the variation of the specific humidity is given below:

$$\frac{d\omega}{dz} = \frac{\rho_g A_s h_m N \left(\omega_{\text{int}} - \omega_g\right)}{\dot{m}_g U_d} \tag{8}$$

where ρ_g is the air density, $\dot{m}_g$ the air mass flow rate, and N the number of droplets entering the humidifier per second, which is calculated from the seawater mass flow rate inflowing the evaporator $\dot{m}_{\text{sw,in}}$ as follows:

$$N = \frac{6\dot{m}_{\text{sw,in}}}{\pi \rho_{\text{sw,in}} D_{d,\text{in}}^3} \tag{9}$$

In order to solve the differential equations listed so far, the humidifier was divided into n differential elements of length Δz and equal volume along the vertical axis, as illustrated in Fig. 2. From an energy balance applied to the gas contained in each element, the following equation results:

$$\dot{m}_g U_d \frac{dh_g}{dz} = \sum_n \left(-h_h A_s \left(T_g - T_d\right) - h_{\text{fg}} U_d \frac{dm_d}{dz} \right) \tag{10}$$

where $\dot{m}_g$ is the gas mass flow rate and h_g is the gas enthalpy. Additionally, from mass and energy balances applied to a whole element, the following equations are derived:

$$\dot{m}_{\text{sw,in}} + \dot{m}_{g,\text{in}} = \dot{m}_{\text{sw,out}} + \dot{m}_{g,\text{out}} \tag{11}$$

$$h_{\text{sw},z} \dot{m}_{\text{sw},z} + h_{g,z} \dot{m}_{g,z} = h_{\text{sw},z+\Delta z} \dot{m}_{l,z+\Delta z} + h_{\text{sw},z+\Delta z} \dot{m}_{g,z+\Delta z} \tag{12}$$

Finally, from a mass balance over the whole evaporator, the total evaporation rate $\dot{m}_{\text{ew}}$ can be found with the next equation:

$$\dot{m}_{\text{ew}} = \dot{m}_a \left(\omega_{\text{out},e} - \omega_{\text{in},e}\right) \tag{13}$$

The solution procedure applied in this work is iterative. The differential equations were discretized by an implicit
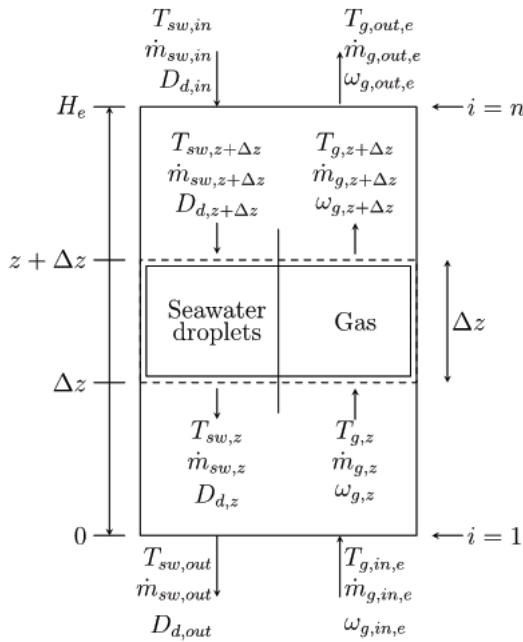
Fig. 2. A differential element in the vertical direction Δz of the humidifier.

finite difference scheme and solved through the finite difference method in the software Matlab. The following assumptions were done:

- Operation occurs at steady-state conditions.
- Horizontal temperature gradients are neglected for all of the substances involved.
- There is no heat transfer to or from the surroundings.
- The air does not experience any compressibility effect.
- The desalination system operates at constant atmospheric pressure. Pressure losses are negligible.
- All the droplets have the same diameter when they enter the evaporator and the condenser.
- The velocity and diameter of the droplets contained in each differential element are constant.
- The gas does not experience any significant change in its properties while going from the humidifier to the dehumidifier or when returning.

In Fig. 2, for the first node, the gas inlet temperature, mass flow rate, and humidity were known. The temperature, mass flow rate, and diameter of the seawater droplets were guessed. The values of the properties required were calculated at the conditions present in the differential volume. After solving the equations, the gas and seawater outlet conditions were determined and used as inlet conditions for the next element. At node n, the temperature, mass flow rate, and diameter of the seawater droplets were calculated and compared with the already known true values; if the differences were considered acceptable (for instance, 0.2°C or 0.5 × 10^{-7} m), the solution procedure was terminated; otherwise, new values at node 1 were estimated and the iterations restarted.

Provided that the dehumidifier operates under the same principle as the humidifier and that has equal geometry, all

of the equations previously described can be used to resolve the dehumidifier too, with the exception of Eq. (13). In Eq. (9), $\dot{m}_{sw,in}$ is changed for $\dot{m}_{fw,in}$, the mass flow rate of freshwater entering the unit, and $\rho_{sw,in}$ is substituted for $\rho_{fw,in}$, which is the density of this water. From a mass balance applied to the condenser, the total evaporation rate or total product freshwater flow rate $\dot{m}_{pw}$ can be calculated as follows:

$$\dot{m}_{pw} = \dot{m}_a \left(\omega_{in,c} - \omega_{out,c} \right)$$ (14)

To evaluate the performance of the desalination system, two parameters were used. The first one is the gain output ratio (GOR), defined as the ratio of the latent heat of vaporization of the freshwater produced (h_{fg}) to the total amount of heat introduced into the whole system ($\dot{Q}_{in}$)[40]:

$$\text{GOR} = \frac{\dot{m}_{pw} h_{fg}}{\dot{Q}_{in}}$$ (15)

The second parameter employed to test the performance of the system was suggested by Niroomand et al. [38] and is the ratio of the product water flow rate to the evaporation rate, denoted here with the symbol η. In mathematical form, it results

$$\eta = \frac{\dot{m}_{pw}}{\dot{m}_{ew}}$$ (16)

The thermodynamic properties required by the described equations were obtained from the library CoolProp [41] for air and freshwater. It is common to use correlations of pure water properties in this type of analyses. The thermodynamic properties of seawater were obtained from the correlations reported by Sharqawy et al. [42] and Nayar et al. [43]. Feedwater salinity was considered constant at 35 g/kg, which is generally assumed as the standard seawater salinity. The effects of salinity variations on the performance of the system were not investigated since it has been reported that the influence of the salinity value on the production of freshwater is not critical [44].

4. Results and discussion

4.1. Validation

To validate the model developed in this work, a comparison was done against the numerical and experimental results published by Franchini et al. [36,37]. They investigated four configurations of an HD desalination system composed of two vertical columns, each with 0.36 m² of cross-sectional area and 2.0 m of height. In the first and second configurations, the humidifier was free from packing materials. In the third and fourth, it was not. Moreover, in the second and fourth configurations, a recuperative heat exchanger was installed at the outlet of the evaporator to recuperate some of the heat carried by the brine. In all of the cases, hot seawater was sprayed from the top of the humidifier, the condenser was a metallic heat exchanger, and the air followed a close loop.

Provided that their first configuration has a humidifier of the same type as the one used in this work, the corresponding

results they published were employed to validate the model developed here for the same cross-sectional area and height. Furthermore, the validation was done at the same nine operating conditions they examined, which correspond to seawater temperatures at the entrance of the humidifier equal to 45°C, 55°C, and 65°C and seawater to air mass flow rate ratios ($\dot{m}_{sw,in}/\dot{m}_{g,in,e}$) of 0.5, 1.0, and 1.5. The temperature and mass flow rate they reported for the seawater were 23°C and 0.135 kg/s, respectively. The results of the validation are shown in Fig. 3, in terms of the ratio of produced freshwater to seawater input ($\dot{m}_{pw}/\dot{m}_{sw,in}$).

According to Fig. 3, the production of freshwater increased with the temperature of seawater at the inlet of the evaporator. Moreover, slightly higher productivities were observed at $\dot{m}_{sw,in}/\dot{m}_{g,in,e}$ ratios of 0.5, contrary to the findings of Franchini et al. [37]. However, as the temperature of the seawater at the inlet was augmented even further, the optimal ratio $\dot{m}_{sw,in}/\dot{m}_{g,in,e} = 1$ they reported was also achieved. It is believed that such dissimilarity is due to the different types of dehumidification principles used here. They employed a conventional heat exchanger while in this work the humid air was cooled by spraying cold water on it, as explained in Section 2. Nonetheless, the major difference in the results was approximately 13%.

In Table 1, there is a comparison between the values of the seawater temperature, air temperature, and air relative humidity, ϕ, measured by Franchini et al. [37] at the exit of the humidifier for the configuration without packing material inside the humidifier and those obtained in the present numerical work. The corresponding operating conditions were $\dot{m}_{sw,in} = 0.135$ kg/s, $T_{sw,in} = 55.4$°C, $T_{g,in,e} = 26.6$°C, $\dot{m}_{g,in,e} = 0.135$ kg/s, and $\phi_{in,e} = 100\%$. It can be noticed that the percentages of discrepancy are marginal, thus enhancing the reliability of the model described here.

From the confidence gained through the results exposed in both Fig. 3 and Table 1, it can be established that the theoretical model presented here is valid for investigating the thermal performance and operational characteristics of the HD desalination system without packing materials, which

Table 1
Comparison between the experimental results of Franchini et al. [37] and the present work for an evaporator without packing material. The conditions of operation were $\dot{m}_{sw,in} = 0.135$ kg/s, $T_{sw,in} = 55.4$°C, $T_{g,in,e} = 26.6$°C, $\dot{m}_{g,in,e} = 0.135$ kg/s, and $\phi_{e,in} = 100\%$

Variable	Franchini et al.	Present work	Difference (%)
$T_{sw,out}$ (°C)	36.8	36.4	1.1
$T_{g,e,out}$ (°C)	40.8	40.1	1.6
$\phi_{e,out}$ (%)	100	100	0.0

is the object of this investigation. The effects on the productivity of freshwater caused by changing the values of different variables of interest will be discussed in the following section. The performance of the system according to Eqs. (15) and (16) is also presented.

4.2. Results

Once the model was validated, it was used to investigate the performance of the system at different operating conditions. The temperature and mass flow rate of seawater entering the evaporator were varied in the ranges 60°C–80°C and 0.2–2 kg/s, respectively. The freshwater temperature and mass flow rate at the inlet of the dehumidifier were kept fixed at 15°C and 0.8 kg/s, respectively. Besides, the temperature and mass flow rate of the air ranged from 15°C to 25°C and 0.2 to 2 kg/s, respectively. The humidifier height H_e was set equal to $L = 1.0$ m; nevertheless, the evaporator-condenser height ratio H_c/H_e was investigated as well in the interval $0.5 \leq H_c/H_e \leq 2.0$. The velocity and diameter of the droplets inside the humidifier and dehumidifier varied from 4 to 7 m/s and 0.6 to 1.0 mm, respectively.

4.2.1. Effect of droplet velocity and diameter

The velocity and diameter of the droplets are two parameters of great interest in the analysis of direct-contact desalination systems without packing material because they determine the total heat and mass transfer area between the fluids and the time of residence inside the columns. Fig. 4 shows the effect of the velocity of the droplets on the productivity of freshwater for three distinct droplet diameters: 0.6, 0.8, and 1.0 mm. These values were chosen because they can be easily obtained with commercially available nozzles and are suitable for future experimental investigations.

From Fig. 4, it becomes evident that for all of the cases, as $U_{d,in}$ increased, $\dot{m}_{pw}$ decreased because the droplets inside both chambers had a shorter residence time; thus, a lower amount of water was evaporated and condensed. It can also be noticed that as the diameter of the droplets was diminished, higher evaporation and condensation rates were achieved, augmenting the freshwater productivity. The reduction of the diameter caused the number of droplets inside the chambers to increase, enlarging the total heat and mass transfer area in consequence.

Fig. 5 illustrates the influence of both the velocity and diameter of the droplets on η. As observed from the trends displayed, η remained below 1.0, indicating that the evaporation rate was larger than the condensation rate for all of
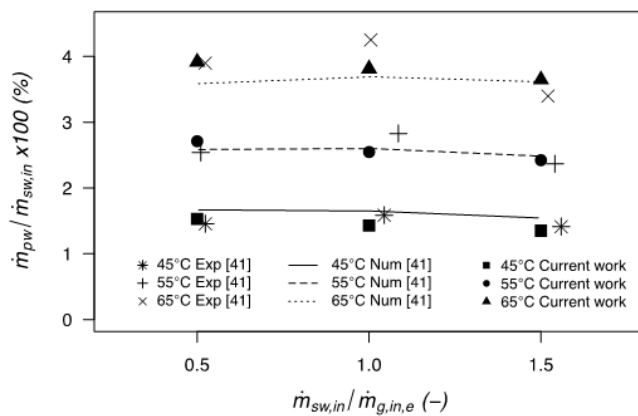

Fig. 3. Model validation using the results published by Franchini et al. [37] at three different seawater temperatures at the entrance of the humidifier and three distinct seawater to air mass flow rate ratios. "Exp" refers to their experimental results and "Num" to their numerical results.
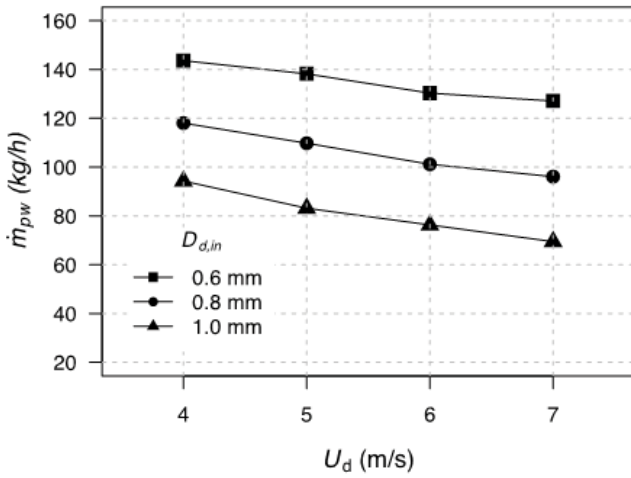
Fig. 4. Effect of the droplet velocity inside the humidifier and dehumidifier on the production of freshwater for different droplet diameters at the entrances (H_e = 1 m, H_c = 1 m, $T_{g,\text{in},e}$ = 20°C, $\dot{m}_{g,\text{in},e}$ = 0.2 kg/s, $\phi_{\text{in},e}$ = 60%, $T_{\text{sw,in}}$ = 80°C, $\dot{m}_{\text{sw,in}}$ = 0.8 kg/s, $T_{\text{fw,in}}$ = 15°C, and $\dot{m}_{\text{fw,in}}$ = 0.8 kg/s).
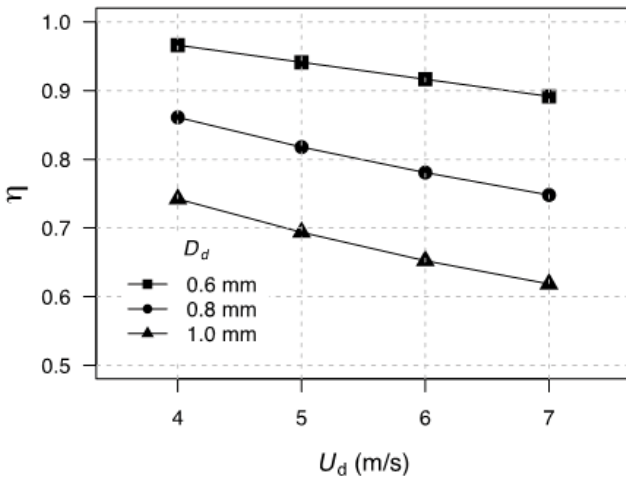
Fig. 5. Effect of the droplet velocity inside the humidifier and dehumidifier on η for different droplet diameters at the inlets (H_e = 1 m, H_c = 1 m, $T_{g,\text{in},e}$ = 20°C, $\dot{m}_{g,\text{in},e}$ = 0.2 kg/s, $\phi_{\text{in},e}$ = 60%, $T_{\text{sw,in}}$ = 80°C, $\dot{m}_{\text{sw,in}}$ = 0.8 kg/s, $T_{\text{fw,in}}$ = 15°C, and $\dot{m}_{\text{fw,in}}$ = 0.8 kg/s).

the cases investigated. It is believed that such behavior was caused by the differences in the temperature and specific humidity gradients inside the humidifier and the dehumidifier. As shown by Eqs. (6) and (8), any change in the droplet diameter and velocity has a direct influence on the mentioned gradients.

4.2.2. Effect of humidifier and dehumidifier heights

The influence of the heights of the humidifier and dehumidifier on the production of freshwater is depicted in Fig. 6, where it can be observed that larger values of H_c promoted a higher productivity since the droplet residence time in the dehumidifier was augmented; therefore, the condensation
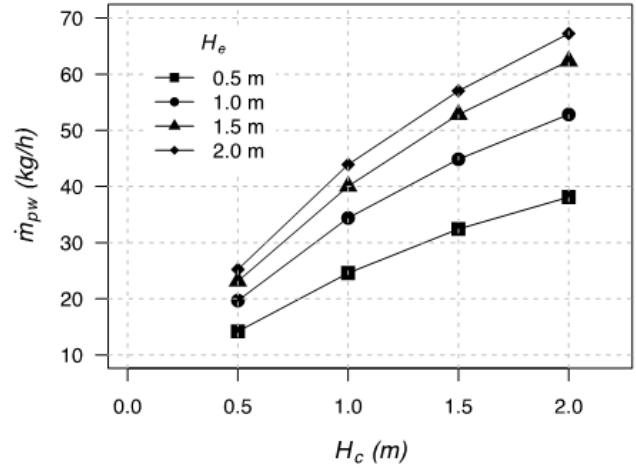

Fig. 6. Effect of the humidifier height on freshwater production at different dehumidifier heights ($D_{d,\text{in}}$ = 1 mm, U_d = 4 m/s, $T_{g,\text{in},e}$ = 20°C, $\dot{m}_{g,\text{in},e}$ = 0.2 kg/s, $\phi_{\text{in},e}$ = 60%, $T_{\text{sw,in}}$ = 80°C, $\dot{m}_{\text{sw,in}}$ = 0.8 kg/s, $T_{\text{fw,in}}$ = 15°C, and $\dot{m}_{\text{fw,in}}$ = 0.8 kg/s).

process was extended and $\dot{m}_{\text{pw}}$ increased. Moreover, the augmentation of H_e was also characterized by larger productivities because for the same parcel of air there was more time available to enlarge its humidity content inside the evaporator. Thus, a larger amount of water was accessible for condensation.

It was also noticed that when H_e was kept constant and H_c was augmented, the magnitude of $\dot{m}_{\text{pw}}$ could be up to 35% larger than the value it had when H_c was kept constant and H_e was enlarged. Therefore, it can be argued that the height of the condenser has a greater impact on $\dot{m}_{\text{pw}}$ than the height of the evaporator. From Fig. 6, it can also be appreciated that as H_e and H_c rose, the corresponding increments of $\dot{m}_{\text{pw}}$ became lower due to the implied reduction of the specific humidity and temperature gradients inside the columns.

4.2.3. Effect of seawater mass flow rate

In Figs. 7(a) and (b), the dependence of freshwater production on the mass flow rate of seawater entering the humidifier for different condenser-evaporator height ratios and droplet diameters of 0.6, and 1.0 mm, respectively, is portrayed. As it can be seen, for any H_c/H_e ratio, $\dot{m}_{\text{pw}}$ showed consistent increasing trends regardless of the diameter of the droplets because the augmentation of $\dot{m}_{\text{sw,in}}$ is always accompanied by an elevation in the number of droplets inside both chambers, as indicated by Eq. (9). Therefore, the total heat and mass transfer area is always enlarged.

From Fig. 7(a), it was noticed that for $D_{d,\text{in}}$ = 0.6 m and $\dot{m}_{\text{sw,in}}$ = 0.5 kg/s, $\dot{m}_{\text{pw}}$ increased less than 1% for $1.5 < H_c/H_e < 2.0$ and less than 5.5% for $1.0 < H_c/H_e < 1.5$. Hence, it does not seem reasonable to build an HD desalination system with a ratio H_c/H_e greater than 1.0 for those operating conditions. The augmentation of the construction expenses is not justified by the extra gain in freshwater production. A similar trend can also be seen for $D_{d,\text{in}}$ = 1.0 m when H_c/H_e exceeded 1.5. This suggests that for a given droplet diameter, there should be an optimum value of H_c/H_e. Beyond it, the gains in freshwater productivity are not justified.
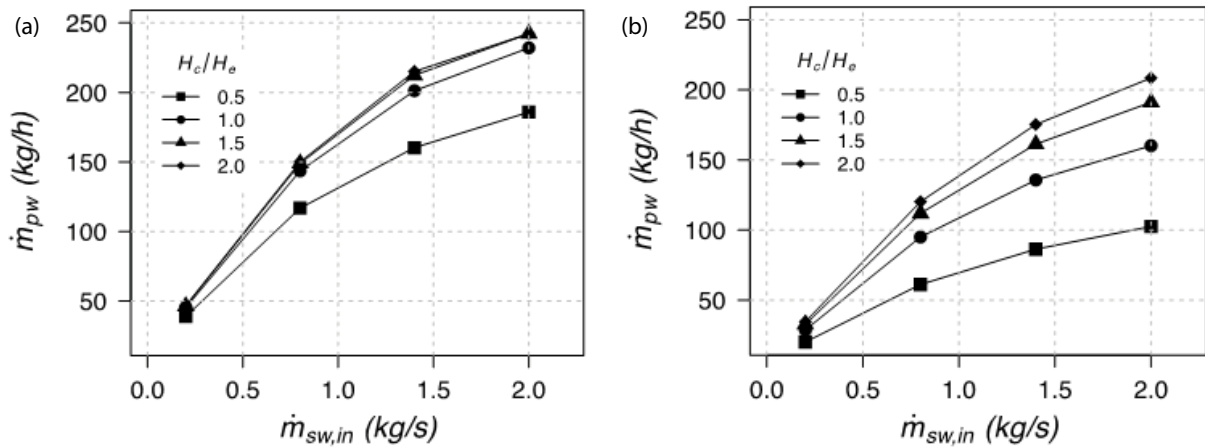
Fig. 7. Effect of seawater mass flow rate on the production of freshwater at different condenser and evaporator height ratios and two droplet diameters: (a) $D_{d,in}$ = 0.6 mm, (b) $D_{d,in}$ = 1.0 mm (H_e = 1 m, U_d = 4 m/s, $T_{g,in,}$ = 20°C, $\dot{m}_{g,in,e}$ = 0.2 kg/s, $\phi_{in,e}$ = 60%, $T_{sw,in}$ = 80°C, $T_{fw,in}$ = 15°C, and $\dot{m}_{fw,in}$ = 0.8 kg/s).

Figs. 8(a) and (b) illustrate the influence of $\dot{m}_{sw,in}$ over η for the same operating conditions of Figs. 7(a) and (b), respectively. From the comparison between both Figs, it can be observed that when $D_{d,in}$ = 0.6 mm, the magnitude of η was higher than its magnitude when $D_{d,in}$ = 1.0 mm, for each H_c/H_e ratio. The reason for this behavior is the fact that for lower droplet diameters, the total area of heat and mass transfer increases. From the figures, it can also be noticed that η was inferior to 1.0 in the majority of the situations. This indicates that as $\dot{m}_{sw,in}$ rises, the performance of the evaporator grows more rapidly than that of the condenser.

4.2.4. Effect of air mass flow rate

In Fig. 9, the variation of the produced freshwater mass flow rate in terms of the air mass flow rate is displayed for distinct height ratios. It can be observed that as $\dot{m}_{g,in,e}$ grew, $\dot{m}_{pw}$ decayed. This is due to the increments of the air velocity because for a given parcel of gas, the time during which the fluids are in contact is reduced. In spite of the fact that

the magnitude of the heat transfer coefficient was increased through augmenting the velocity, the decreasing tendency of $\dot{m}_{pw}$ was not stopped. Furthermore, it was noticed that larger values of $\dot{m}_{g,in,e}$ caused higher specific humidity contents at the exit of the condenser.

From the same figure, it was also noticed that by augmenting the height ratio, the production of freshwater improved; nevertheless, for ratios larger than 1.0 at $\dot{m}_{g,in,e}$ < 0.5 kg/s or larger than 1.5 for $\dot{m}_{g,in,e}$ < 2.0 kg/s, the benefits were marginal. For instance, at $\dot{m}_{g,in,e}$ = 0.2 kg/s, the gains in $\dot{m}_{pw}$ for H_c/H_e > 1.0 were inferior to 4.0%. Therefore, the use of relatively high H_c/H_e values may not be beneficial in terms of the freshwater production. Fig. 10 shows the effect of $\dot{m}_{g,in,e}$ over the ratio η for the same conditions as Fig. 9.

According to the tendencies displayed in Fig. 10, it can be seen that the decreasing behavior exhibited by η as $\dot{m}_{g,in,e}$ augmented was similar to that of Fig. 9, though the decrements were more drastic in this case. This demonstrates that the temperature and specific humidity gradients inside the dehumidifier are significantly affected by a low residence
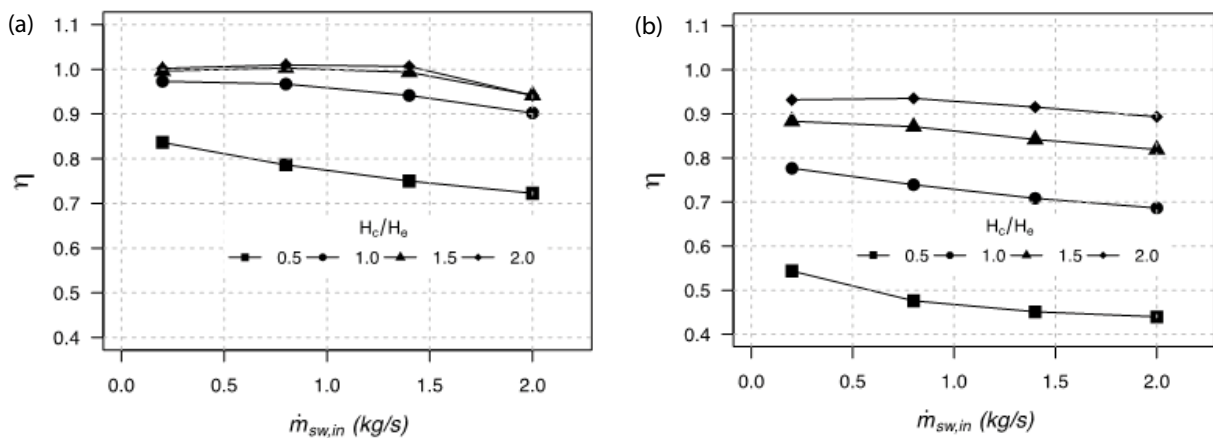

Fig. 8. Effect of seawater mass flow rate on η at different condenser and evaporator height ratios and two droplet diameters: (a) $D_{d,in}$ = 0.6 mm, (b) D_d = 1.0 mm (H_e = 1 m, U_d = 4 m/s, $T_{g,in,e}$ = 20°C, $\dot{m}_{g,in,e}$ = 0.2 kg/s, $\phi_{in,e}$ = 60%, $T_{sw,in}$ = 80°C, $T_{fw,in}$ = 15°C, and $\dot{m}_{fw,in}$ = 0.8 kg/s).
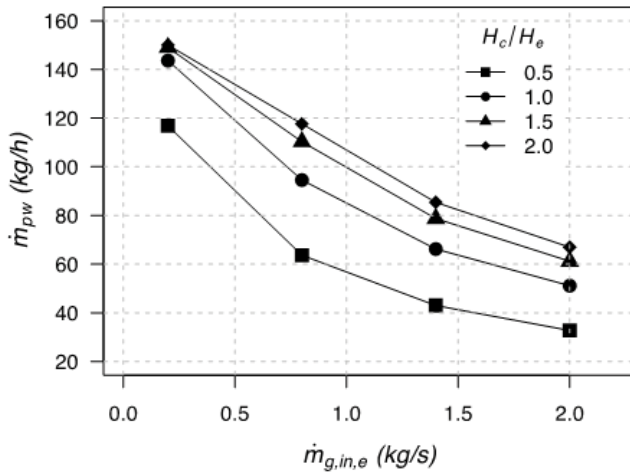
Fig. 9. Effect of air mass flow rate on the production of freshwater at different condenser and evaporator height ratios (H_e = 1 m, $D_{d,in}$ = 0.6 mm, U_d = 4 m/s, $T_{g,in,e}$ = 20°C, $\phi_{in,e}$ = 60%, $T_{sw,in}$ = 80°C, and $\dot{m}_{sw,in}$ = 0.8 kg/s, $T_{fw,in}$ = 15°C, and $\dot{m}_{fw,in}$ = 0.8 kg/s).
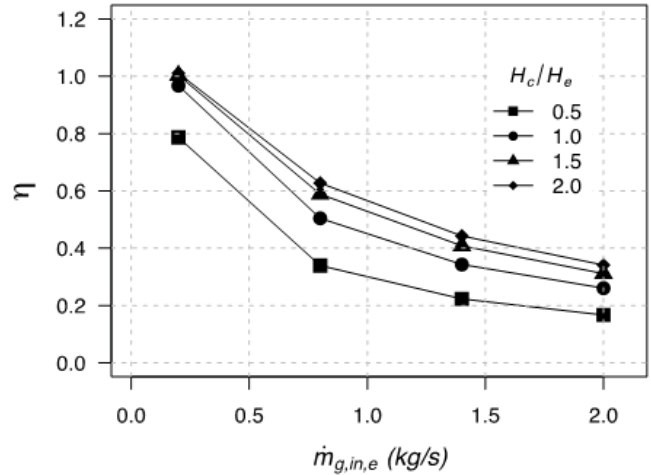
Fig. 10. Effect of the air mass flow rate over η at different condenser and evaporator height ratios (H_e = 1 m, $D_{d,in}$ = 0.6 mm, U_d = 4 m/s, $T_{g,in,e}$ = 20°C, $\phi_{in,e}$ = 60%, $T_{sw,in}$ = 80°C, $\dot{m}_{sw,in}$ = 0.8 kg/s, $T_{fw,in}$ = 15°C, and $\dot{m}_{fw,in}$ = 0.8 kg/s).

time of the air in the humidifier because the content of water vapor during the evaporation process cannot be substantially improved. As in the previous graph, it can be observed here that the increment of the height ratio also had a beneficial effect. However, beyond $H_c/H_e > 1.5$, the gains were minimal, especially at low air mass flow rates.

4.2.5. Effect of seawater temperature

In Fig. 11, the influence that the seawater temperature entering the humidifier has on $\dot{m}_{pw}$ and η is displayed for different values of H_c/H_e. It can be noticed from Fig. 11(a) that as $T_{sw,in}$ increased, $\dot{m}_{pw}$ augmented because a large value of $T_{sw,in}$ is beneficial for the processes of heat and mass transfer between the fluids inside the evaporator. Nevertheless, the effect of $T_{sw,in}$ on η was not significant (Fig. 11(b)). For any fixed magnitude of H_c/H_e, the improvement of η between consecutive seawater temperatures never surpassed 1.4% in all of the cases.

Fig. 12 shows the variation of the seawater droplets and air temperatures in the humidifier for two values of $T_{sw,in}$. It can be observed that the temperature difference between both fluids in the evaporator was larger at the base of the column and then it decreased gradually. A difference equal to zero was never reached. The benefit of a higher $T_{sw,in}$ is explained by the existence of a greater temperature difference which favors convection heat transfer. Moreover, it also implies a higher value of the enthalpy of vaporization of the seawater droplets which positively influences the magnitude of ω_{int}, enhancing the mass transfer according to Eq. (1). Such benefit can be appreciated in Fig. 13 where the variation of the humidity ratio throughout the humidifier is plotted for two values of $T_{sw,in}$.

4.2.6. Effect of air inlet temperature

The effect of the air temperature at the inlet of the evaporator on $\dot{m}_{pw}$ is shown in Fig. 14. It was noticed that for a given
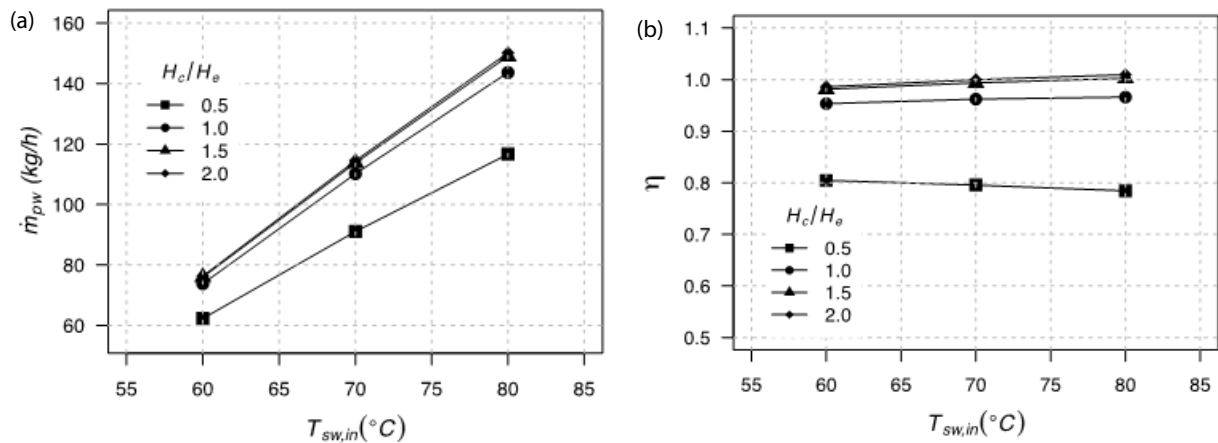

Fig. 11. Effect of the inlet seawater temperature on $\dot{m}_{pw}$ (a) and on η (b) at different height ratios (H_e = 1 m, $D_{d,in}$ = 0.6 mm, U_d = 4 m/s, $T_{g,in,e}$ = 20°C, $\dot{m}_{g,in,e}$ = 0.2 kg/s, $\phi_{in,e}$ = 60%, $\dot{m}_{sw,in}$ = 0.8 kg/s, $T_{fw,in}$ = 15°C, and $\dot{m}_{fw,in}$ = 0.8 kg/s).
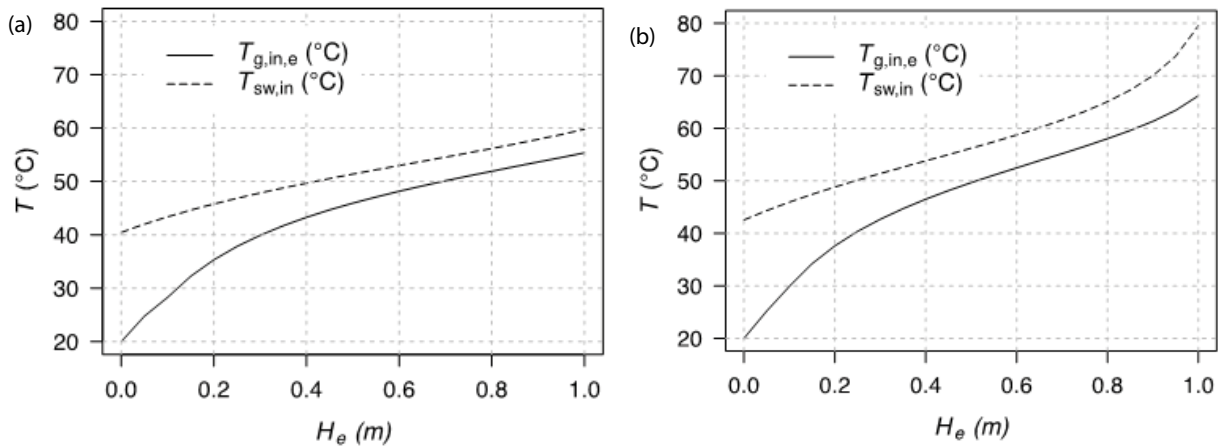
Fig. 12. Variation of the seawater droplets and air temperatures along the height of the humidifier for two values of the inlet seawater temperature: (a) $T_{sw,in} = 60°C$, (b) $T_{sw,in} = 80°C$ ($H_e = 1$ m, $H_c = 1$ m, $D_{d,in} = 0.6$ mm, $U_d = 4$ m/s, $T_{g,in,e} = 20°C$, $\dot{m}_{g,in,e} = 0.2$ kg/s, $\phi_{in,e} = 60$, $\dot{m}_{sw,in} = 0.8$ kg/s, $T_{fw,in} = 15°C$, and $\dot{m}_{fw,in} = 0.8$ kg/s).
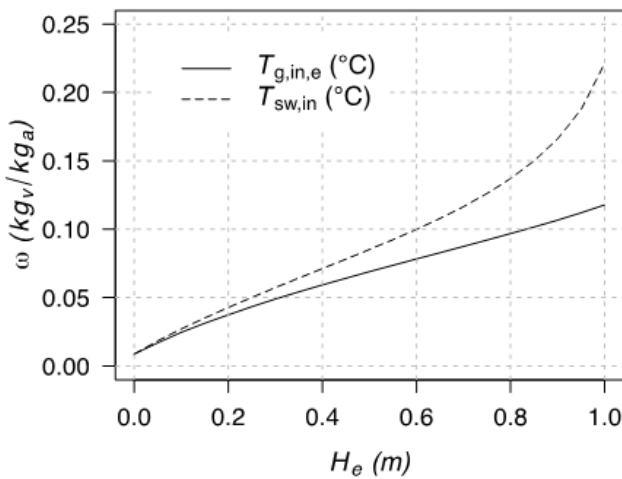

Fig. 13. Variation of the specific humidity ratio throughout the humidifier for two values of the inlet seawater temperature ($H_e = 1$ m, $H_c = 1$ m, $D_{d,in} = 0.6$ mm, $U_d = 4$ m/s, $T_{g,in,e} = 20°C$, $\dot{m}_{g,in,e} = 0.2$ kg/s, $\phi_{in,e} = 60\%$, $T_{sw,in} = 80°C$, $\dot{m}_{sw,in} = 0.8$ kg/s, $T_{fw,in} = 15°C$, and $\dot{m}_{fw,in} = 0.8$ kg/s).

Fig. 14. Effect of air inlet temperature on $\dot{m}_{pw}$ for different height ratios ($D_d = 0.6$ mm, $U_d = 4.0$ m/s, $H_e = 1.0$ m, $T_{sw,in,e} = 80°C$, $\dot{m}_{sw,in,e} = 0.8$ kg/s, $T_{fw,in,c} = 15°C$, $\dot{m}_{fw,in,c} = 0.8$ kg/s, $\dot{m}_{g,in,e} = 0.2$ kg/s, and $\phi_{g,in,e} = 60\%$).

value of H_c/H_e, the increment in $\dot{m}_{pw}$ caused by augmenting $T_{g,in,e}$ was barely visible. For instance, the largest augmentation of $\dot{m}_{pw}$ obtained for an increment of 10°C in the air inlet temperature was 1.3%. On the other hand, from the plots displayed, it is recognizable that an increment of the height ratio is more advantageous, though not for values of H_c/H_e larger than 1.5. The reason for the marginal effect caused by $T_{g,in,e}$ can be explained using Fig. 15, where the variation of the air temperature inside the evaporator is depicted for three different values of $T_{g,in,e}$.

As it can be seen from Fig. 15, after approximately 0.3 m above the bottom of the humidifier, the gaps amid the curves narrowed considerably. It seems that the air temperature inside the evaporator rose following almost the same pattern, both in shape and magnitude. It is thought that for higher values of the air inlet temperature, a noticeable gap can still
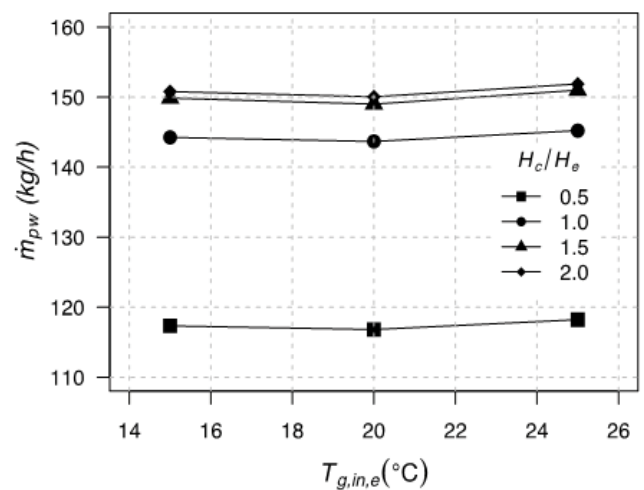
be observed at a larger distance above the bottom of the column; however, a similar growing trend of $T_{g,e}$ is expected without significant augmentations in the productivity of desalinated water.

The effect of $T_{g,in,e}$ on η can be observed in Fig. 16, where relevant increments were detected for $0.5 < H_c/H_e < 1.5$. Unlike Fig. 14, the increase in η for a given height ratio was in this case more pronounced because the relative humidity at the evaporator inlet was fixed at 60%. This implies that the specific humidity of the entering air grew as $T_{g,in,e}$ augmented. Therefore, despite the fact that the temperature gradient between the fluids inside the humidifier was reduced, the water vapor content in the air at the exit of the column was larger. Furthermore, as $H_c/H_e \geq 1.0$ and $T_{g,in,e} \geq 20°C$, η was greater than 1.0, suggesting that at these conditions, some of the water vapor contained in the air before it entered
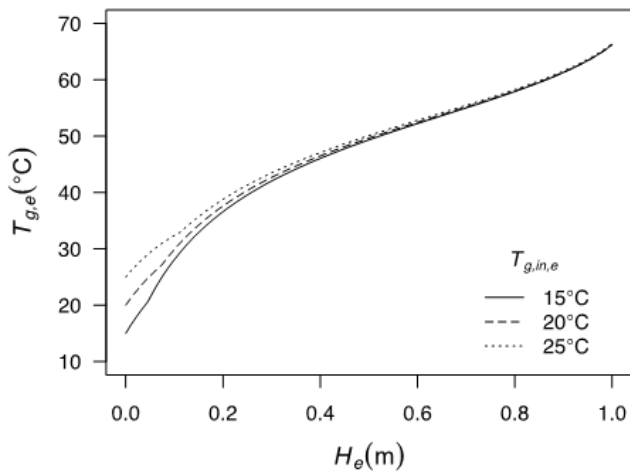
Fig. 15. Variation of the air temperature inside the humidifier for three values of the air inlet temperature (D_d = 0.6 mm, U_d = 4.0 m/s, H_c = 1.0 m, H_e = 1.0 m, $T_{sw,in,e}$ = 80°C, $\dot{m}_{sw,in,e}$ = 0.8 kg/s, $T_{fw,in,c}$ = 15°C, $\dot{m}_{sw,in,e}$ = 0.8 kg/s, $\dot{m}_{g,in,e}$ = 0.2 kg/s, and $\phi_{g,in,e}$ = 60%).
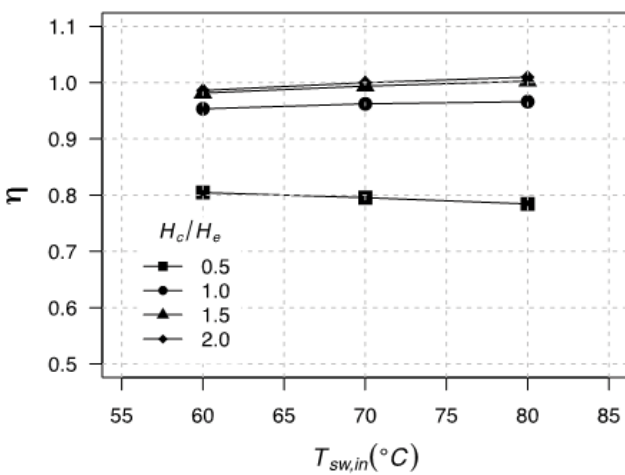

Fig. 16. Effect of air temperature on η at distinct humidifier and dehumidifier height ratios (D_d = 0.6 mm, U_d = 4.0 m/s, H_e = 1.0 m, $T_{sw,in,e}$ = 80°C, $\dot{m}_{sw,in,e}$ = 0.8 kg/s, $T_{fw,in,c}$ = 15°C, $\dot{m}_{fw,in,c}$ = 0.8 kg/s, $\dot{m}_{g,in,e}$ = 0.2 kg/s, and $\phi_{g,in,e}$ = 60%).

the humidifier was also condensed, thus enhancing the productivity.

4.3. Gained output ratio

The performance of the HD desalination system is described in this section. In Fig. 17, the variation of the GOR in terms of the mass flow rate ratio $\dot{m}_{pw}/\dot{m}_{g,in,e}$ is shown for the four height ratios H_c/H_e investigated. A rising trend as the ratio $\dot{m}_{pw}/\dot{m}_{g,in,e}$ increased was observed. Given the fact that the produced freshwater varied inversely to the air mass flow rate, as depicted in Fig. 9, the largest values of GOR occurred at the smallest values of $\dot{m}_{g,in,e}$ for the four height ratios. They were 0.48, 0.56, 0.57, and 0.58, respectively. It can also be noticed that for $H_c/H_e > 1.5$, the increments of GOR were not substantial.

In the plots of Fig. 17, it can be seen that for every H_c/H_e, the last point of the corresponding curve is considerably far
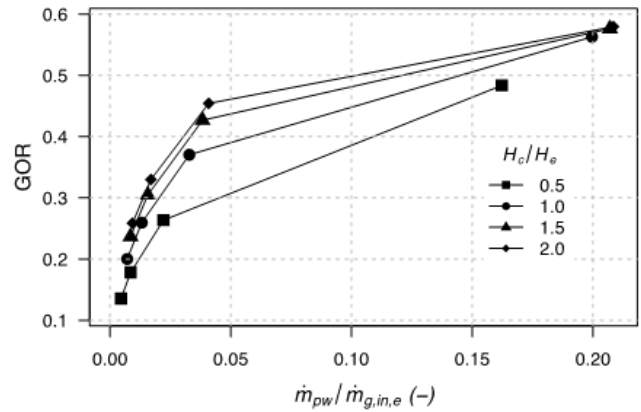

Fig. 17. Variation of the GOR as a function of the mass flow rate ratio $\dot{m}_{pw}/\dot{m}_{g,in,e}$ for four condenser and evaporator height ratios (H_e = 1 m, $D_{d,in}$ = 0.6 mm, U_d = 4 m/s, $T_{g,in,e}$ = 20°C, $\phi_{in,e}$ = 60%, $T_{sw,in}$ = 80°C, $\dot{m}_{sw,in}$ = 0.2 kg/s $T_{fw,in}$ = 15°C, and $\dot{m}_{fw,in}$ = 0.8 kg/s).

from the previous point. The reason for this behavior is the significant decay in the production of freshwater when the mass flow rate of air entering the evaporator augmented from 0.2 to 0.6 kg/s, as illustrated in Fig. 9. The low values obtained for the GOR exemplify the necessity of recovering part of the heat that is carried by the brine out of the evaporator or by the air leaving the condenser. If the recovered heat is used to preheat the seawater, less energy from an external source will be required and the performance will be improved.

Provided that the work of Franchini et al. [36,37] was employed to validate the mathematical model presented here, it seemed natural to compare the values of the GOR at the same conditions of validation (Table 1). Using the data they reported, for the configuration with packing inside the humidifier, the GOR was 1.15, whereas for the configuration without packing in the humidifier, it was 0.96. The GOR given by the model developed here at those conditions was 0.40. The reason for the difference is the fact that by employing a metallic heat exchanger in the condenser, they used the heat of the air to preheat the seawater sent to the evaporator. Had they not used such an arrangement, the values of the GOR would have been 0.64 with packing in the humidifier and 0.53 without packing.

A second reason for the higher GOR of the desalination system proposed by Franchini et al. [36,37], even for the hypothetical conditions in which the feedwater were not preheated, is the fact that for the conditions of operation investigated, the use of a metallic heat exchanger as condenser seemed to be more suitable than the direct-contact dehumidification system used in the present work. Nonetheless, the benefit might not be significant enough to overcome the negative issues associated with metallic heat exchangers, such as pressure drop, fouling and corrosion, as well as the extra investment costs.

5. Conclusions

A numerical investigation was developed to study the thermal performance and operational characteristics of a humidifier-dehumidifier seawater desalination system where both the evaporator and the condenser do not have filling

materials. For a given geometry of the system, the parameters which affect the production of freshwater the most were the feedwater mass flow rate and temperature and the size and velocity of the droplets in the evaporator and condenser. The benefit of heating the air before entering the humidifier was marginal, and the increment of the air mass flow rate was in general adverse. The following are the main conclusions:

- The largest production of freshwater achieved was 242.2 kg/h, at H_c/H_e = 2.0, corresponding to the smallest diameter and velocity of the droplets ($D_{d,in}$ = 0.6 mm, U_d = 4.0 m/s) and to the largest seawater mass flow rate and temperature at the entrance of the humidifier ($\dot{m}_{sw,in}$ = 2.0 kg/s, $T_{sw,in}$ = 80°C).
- Increasing the condenser-evaporator height ratio H_c/H_e in general had a positive effect on the production of freshwater. However, beyond H_c/H_e = 1.5, the benefit was not significant. For instance, when rising from 1.5 to 2.0 at the same conditions of the previous bullet, the gain was only 4.4%, which may not be worthy of the additional investment in materials.
- For all the cases investigated, the values of the GOR were considerably low. The largest value obtained was 0.58. It is believed that the use of packing materials inside the humidifier can improve the performance; nevertheless, more substantial improvements could be achieved if schemes of heat recovery were integrated into the desalination system.

Symbols

A	—	Area, m^2
Cp	—	Specific heat of air, kJ/kg K
D	—	Diameter, m
GOR	—	Gain output ratio, –
H	—	Height, m
h	—	Specific enthalpy, kJ/kg
h_{fg}	—	Latent heat of evaporation, kJ/kg
h_h	—	Heat transfer coefficient, W/m^2 K
h_m	—	Mass transfer coefficient, m/s
i	—	Node number, –
L	—	Length, m
m	—	Mass, kg
$\dot{m}$	—	Mass flow rate, kg/s
n	—	Number of differential elements, –
N	—	Number of droplets per second, 1/s
Nu	—	Nusselt number, –
Pr	—	Prandtl number, –
$\dot{Q}$	—	Heat flux, kJ/s
Re	—	Reynolds number, –
Sc	—	Schmidt number, –
Sh	—	Sherwood number, –
T	—	Temperature, °C
U	—	Velocity, m/s
W	—	Relative velocity, m/s
z	—	Vertical coordinate axis, m

Greek

α	—	Diffusivity, m^2/s
η	—	Efficiency, –
λ	—	Thermal conductivity, kW/m K
μ	—	Dynamic viscosity, Pa s
ν	—	Kinetic viscosity, m^2/s
ρ	—	Density, kg/m^3
ω	—	Specific humidity (kg water vapor/kg dry air)

Subscripts

a	—	Dry air
c	—	Condenser
d	—	Droplet
e	—	Evaporator
ew	—	Evaporation rate
fw	—	Freshwater
g	—	Mixture of air and water vapor
in	—	Inlet
int	—	Interphase
out	—	Outlet
pw	—	Production or condensation rate
s	—	Surface
sw	—	Seawater
v	—	Vapor
w	—	Water

References

[1] WWAP, (United Nations World Water Assessment Programme), Technical report, The United Nations World Water Development Report 2018: Nature-based Solutions, UNESCO, Paris, 2018.

[2] WWAP, (United Nations World Water Assessment Programme), Technical report, The United Nations World Water Development Report 2015: Water for a Sustainable World, UNESCO, Paris, 2015.

[3] H.M. Qiblawey, F. Banat, Solar thermal desalination technologies, Desalination, 220 (2008) 633–644.

[4] M.M. Naim, M.A. Abd El Kawi, Non-conventional solar stills Part 1. Non-conventional solar stills with charcoal particles as absorber medium, Desalination, 153 (2003) 55–64.

[5] X. Li, G. Yuan, Z. Wang, H. Li, Z. Xu, Experimental study on a humidification and dehumidification desalination system of solar air heater with evacuated tubes, Desalination, 351 (2014) 1–8.

[6] M. Chandrashekara, A. Yadav, Water desalination system using solar heat: a review, Renew. Sust. Energ. Rev., 67 (2017) 1308–1330.

[7] J.H. Reif, W. Alhalabi, Solar-thermal powered desalination: its significant challenges and potential, Renew. Sust. Energ. Rev., 48 (2015) 152–165.

[8] S.M. Shalaby, Reverse osmosis desalination powered by photovoltaic and solar ran- kine cycle power systems: a review, Renew. Sust. Energ. Rev., 73 (2017) 789–797.

[9] Y. Zhang, M. Sivakumar, S. Yang, K. Enever, M. Ramezanianpour, Application of solar energy in water treatment processes: a review, Desalination, 428 (2018) 116–145.

[10] V.G. Gude, Energy storage for desalination processes powered by renewable energy and waste heat sources, Appl. Energy, 137 (2015) 877–898.

[11] T. Chung, S. Zhang, K.Y. Wang, J. Su, M.M. Ling, Forward osmosis processes: yesterday, today and tomorrow, Desalination, 287 (2012) 78–81.

[12] T.Y. Cath, A.E. Childress, M. Elimelech, Forward osmosis: Principles, applications, and recent developments, J. Membr. Sci., 281 (2006) 70–87.

[13] S.M. Shalaby, M.A. Bek, A.E. Kabeel, Design recommendations for humidification-dehumidification solar water desalination systems, Energy Procedia, 107 (2017) 270–274.

[14] M.B. Amara, I. Houcine, A. Guizani, M. Maalej, Experimental study of a multiple-effect humidification solar desalination technique, Desalination, 170 (2004) 209–221.

[15] X. Li, S. Muraleedaaran, L. Li, R. Lee, A humidification-dehumidification process for produced water purification, Desal. Wat. Treat., 20 (2010) 51–59.

[16] C. Chiranjeevi, T. Srinivas, Influence of vapor absorption cooling on humidification-dehumidification (hdh) desalination, Alexandria Eng. J., 55 (2016) 1961–1967.

[17] S. Parekh, M.M. Farid, J.R. Selman, S. Al-Hallaj, Solar desalination with a humidification-dehumidification technique — a comprehensive technical review, Desalination, 160 (2004) 167–186.

[18] A.E. Kabeel, M.H. Hamed, Z.M. Omara, S.W. Sharshir, Water desalination using a humidification-dehumidification technique — a detailed review, Nat. Resour., 4 (2013) 286–305.

[19] M.A. Jamil, S.M. Elmutasim, S.M. Zubair, Exergo-economic analysis of a hybrid humidification dehumidification reverse osmosis (HDH-RO) system operating under different retrofits, Energy Convers. Manage., 158 (2018) 286–297.

[20] S.W. Sharshir, G. Peng, N. Yang, M.O.A. El-Samadony, A.E. Kabeel, A continuous desalination system using humidification – dehumidification and a solar still with an evacuated solar water heater, Appl. Therm. Eng., 104 (2016) 734–742.

[21] S.W. Sharshir, G. Peng, N. Yang, M.A. Eltawil, M.K.A. Ali, A.E. Kabeel, A hybrid desalination system using humidification-dehumidification and solar stills integrated with evacuated solar water heater, Energy Convers. Manage., 124 (2016) 287–296.

[22] A.S. Abdullah, F.A. Essa, Z.M. Omara, M.A. Bek, Performance evaluation of a humidification-dehumidification unit integrated with wick solar stills under different operating conditions, Desalination, 441 (2018) 52–61.

[23] E.M.S. El-Said, A.E. Kabeel, M. Abdulaziz, Theoretical study on hybrid desalination system coupled with nano-fluid solar heater for arid states, Desalination, 386 (2016) 84–98.

[24] W.F. He, D. Han, W.P. Zhu, C. Ji, Thermo-economic analysis of a water-heated humidification-dehumidification desalination system with waste heat recovery, Energy Convers. Manage., 160 (2018) 182–190.

[25] M.H. Hamed, A.E. Kabeel, Z.M. Omara, S.W. Sharshir, Mathematical and experimental investigation of a solar humidification–dehumidification desalination unit, Desalination, 358 (2015) 9–17.

[26] A.E. Kabeel, M. Abdelgaied, Experimental evaluation of a two-stage indirect solar dryer with reheating coupled with HDH desalination system for remote areas, Desalination, 425 (2018) 22–29.

[27] A.E. Kabeel, M. Abdelgaied, Y. Zakaria, Performance evaluation of a solar energy assisted hybrid desiccant air conditioner integrated with HDH desalination system, Energy Convers. Manage., 150 (2017) 382–391.

[28] W.F. He, D. Han, C. Ji, Investigation on humidification dehumidification desalination system coupled with heat pump, Desalination, 436 (2018) 152–160.

[29] G. Yuan, Z. Wang, H. Li, X. Li, Experimental study of a solar desalination system based on humidification–dehumidification process, Desalination, 277 (2011) 92–98.

[30] M. Mehrgoo, M. Amidpour, Constructal design and optimization of a direct contact humidification–dehumidification desalination unit, Desalination, 293 (2012) 69–77.

[31] M.H. Sharqawy, M.A. Antar, S.M. Zubair, A.M. Elbashir, Optimum thermal design of humidification dehumidification desalination systems, Desalination, 349 (2014) 10–21.

[32] A.E. Kabeel, E.M.S. El-Said, Technological aspects of advancement in low-capacity solar thermal desalination units, Int. J. Sust. Energ., 32 (2013) 315–332.

[33] Y.B. Karhe, P.V. Walke, A solar desalination system using humidification- dehumidification process - A review of recent research, Int. J. Mod. Eng. Res., 3 (2013) 962–969.

[34] W. Abdelmoez, M.S. Mahmoud, T.E. Farrag, Water desalination using humidification/dehumidification (hdh) technique powered by solar energy: a detailed review. Desal. Wat. Treat., 52 (2014) 4622–4640.

[35] A. Giwa, N. Akther, A.A. Housani, S. Haris, S.W. Hasan, Recent advances in humidification dehumidification (HDH) desalination processes: improved designs and productivity, Renew. Sust. Energ. Rev., 57 (2016) 929–944.

[36] G. Franchini, A. Perdichizzi, Modeling of a solar driven HD (humidification-dehumidification) desalination system, Energy Procedia, 45 (2014) 588–597.

[37] G. Franchini, L.E. Padovan, A. Perdichizzi, Design and construction of a desalination prototype based on HD (humidification-dehumidification) process, Energy Procedia, 81 (2015) 472–481.

[38] N. Niroomand, M. Zamen, M. Amidpour, Theoretical investigation of using a direct contact dehumidifier in humidification-dehumidification desalination unit based on an open air cycle, Desal. Wat. Treat., 54 (2015) 305–315.

[39] W.E. Ranz, W.R. Marshall, Evaporation from drops, Chem. Eng. Prog., 48 (1952) 141–180.

[40] S.M. Elmutasim, M.A. Ahmed, M.A. Antar, P. Gandhidasan, S.M. Zubair, Design strategies of conventional and modified closed-air open- water humidification dehumidification systems, Desalination, 435 (2018) 114–127.

[41] I.H. Bell, J. Wronski, S. Quoilin, V. Lemort, Pure and pseudopure fluid thermophysical property evaluation and the open-source thermophysical property library coolprop, Ind. Eng. Chem. Res., 53 (2014) 2498–2508.

[42] M.H. Sharqawy, J.H. Lienhard V, S.M. Zubair, Thermophysical properties of seawater: a review of existing correlations and data, Desal. Wat. Treat., 16 (2010) 354–380.

[43] K.G. Nayar, M.H. Sharqawy, L.D. Banchik, J.H. Lienhard V, Thermophysical properties of seawater: A review and new correlations that include pressure dependence, Desalination, 390 (2016) 1–24.

[44] A.E. Kabeel, E.M.S. El-Said, A hybrid solar desalination system of air humidification-dehumidification and water flashing evaporation: Part I. A numerical investigation, Desalination, 320 (2013) 56–72.